A R C H I V E S O F M E T A L L U R G Y A N D M A T E R I A L S
Volume 58 2013 Issue 4
DOI: 10.2478/amm-2013-0136

M. HOJNY*

THERMO-MECHANICAL MODEL OF A TIG WELDING PROCESS FOR THE AIRCRAFT INDUSTRY

MODEL TERMO-MECHANICZNY PROCESU SPAWANIA TIG DLA PRZEMYSŁU LOTNICZEGO

TIG welding is the most important process, which is used in the aircraft industry. A number of components of airplane are made using this method. Thermo-mechanical models are needed to understand better phenomena involved in this process. In the presented work thermo-mechanical simulations were performed and the possibilities of welding distortion in the investigated process were evaluated. Comparison of the results of numerical simulation with the experimental data confirmed good predictive capabilities of the model and quite good description of the phenomena involved in this process.

Keywords: deformations, welding, finite element modeling, Inconel 625 alloy

Spawanie metodą TIG jest jedną z ważniejszych metod używanych w przemyśle lotniczym. Wiele komponentów samolotu powstaje dzięki tej metodzie. Model termo-mechaniczny wspomnianego procesu jest konieczny do dokładnej analizy zjawisk powstających podczas procesu. W prezentowanej pracy opracowano model termo-mechaniczny w kontekście analizy deformacji spawanych elementów. Porównanie otrzymanych wyników na drodze symulacji z wynikami eksperymentalnymi wykazało poprawne odwzorowanie zjawisk zachodzących podczas procesu spawania.

1. Introduction

Permanent technological progress and still growing industrial competition bring a lot of changes in aircraft technology. Predominant processes are drawing technology of metals among them: stamping with elastic die [1], hot forming [3], shear/spinning forming, and so on, as well as casting [2] and welding technology [4]. During welding e.g. Inconel 625 alloy, the heat source leads to rapid heating and melting of the material and the formation of a weld pool that subsequently cools and solidifies. Welding process create numerous internal stresses in welded materials [5]. Welding stresses arise due to the inhomogeneous cooling, and in alloys these stresses are caused by the effect of non-uniformly distributed cooling contractions and solid state phase transformations. As a result, a large deformation of welded assemblies can cause the cracks propagation during welding operation. Modelling of the welding stresses and associated deformations requires a finite element solver able to predict both the thermo-metallurgical and the mechanical development during the process. Finite element solver should account for a series of phenomena such as the material deposition, melting and solidification, solid-state phase transformation, weld arc heat input, the flow stress dependency on the specific mixture of phases appearing at the different temperatures. The main idea of an ideally modeling framework is presented in Fig.1. A thermal, a microstructure and a mechanical sub-model are coupled sequentially. Microstructure based on temperature evolution. Distortions and stresses are influenced both by thermal expansion/contractions and by the flow stress dependent both on temperature and the microstructure – quantified by the strength parameters S_p and S_{GP} [6]. The strength parameters S_p and S_{GP} are output from the microstructure model.

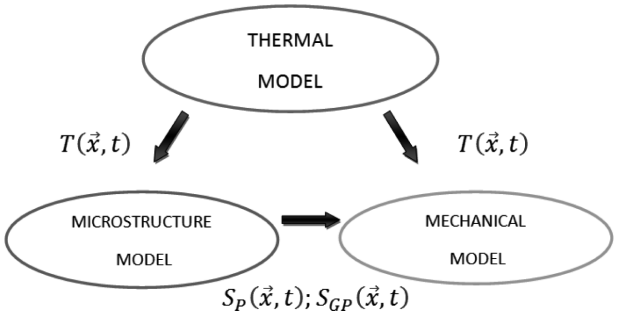

Fig. 1. Modelling framework of welding process

Due to this complexity, simplified models are often applied. This means that numerical models should be carefully validated against controlled experiments before being used to predict welding stresses in real industrial processes. This inspired the author of the present work to make analysis of possibilities of numerical simulations of the TIG (Tungsten Inert Gas) process, which is welding process often used in the aircraft industry. Prediction of the distortion are the main objective of the work. Computer simulations are made by using commercial solver WeldsimS [7] feedback with inverse tool

* AGH UNIVERSITY OF SCIENCE AND TECHNOLOGY, AL. A. MICKIEWICZA 30, 30-059 KRAKÓW, POLAND

(*DEFFEM|inverse module*) included in Extra-High Temperature Solutions Platform (*EHTS Platform*) developed by author. The Extra-High Temperature Solutions Platform (EHTS Platform) has been developed in order to support modelling of plastic deformation of materials at very high temperature levels. WeldsimS is a finite element code developed by Institute for Energy Technology, Kjeller in Norway specialized in simulations of welding processes. It consists of a thermal, a micro-structure and a mechanical sub-model, that are coupled sequentially. By coupling the thermal solver to a micromechanical model several parameters such as yield stress distribution in the HAZ can be determined. Chapter 2 of the paper presents the welding case and the experimental details. The numerical model is summarized in Chapter 3. The modelling results are presented and compared to the experimental results in Chapter 4.

2. Experimental tests

The experiments conducted in the presented work are single pass welding on an Inconel 625 alloy plate, carried out at the WSK "PZL-Rzeszow" S.A., Poland. The main task of these experiments was to evaluate the strain and stresses distribution in the part during TIG welding process. The TIG is an arc welding process that uses a non-consumable tungsten electrode to produce the weld. The weld area is protected from atmospheric exposure by an inert shielding gas. Filler materials can be also used in the TIG process. Their application is depended on element thickness, type of joint and so on. In practice, the filler material is usually the same as the base material. An example scheme of the TIG process is presented in Fig. 2.

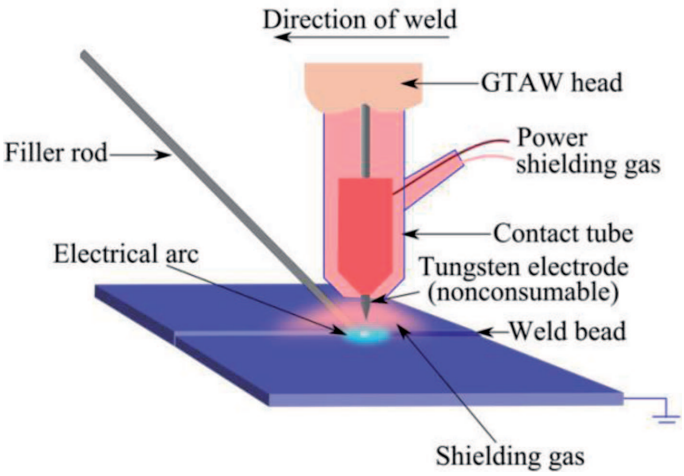

Fig. 2. The scheme of the TIG (GTAW) process

The sample geometry of plate used in the experiment is shown in Fig. 3. It is 50 mm wide, 0.76 mm thick, and 75 mm long in the welding direction. The weld line is marked in Fig. 3 with dashed line.

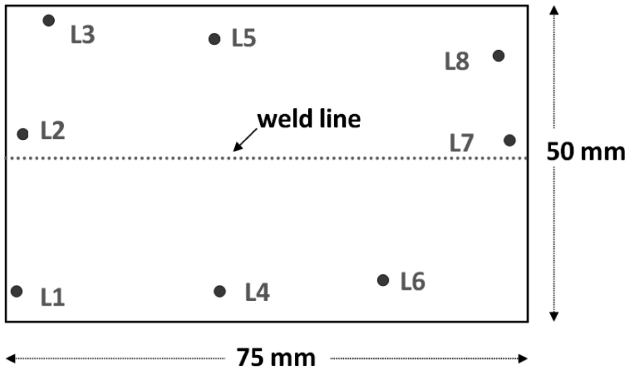

Fig. 3. Sample geometry and the location of the various log points (L1-L8)

In order to measure deformation after welding process, the industrial high-end 3D digitizer was used. The measurements were performed at ITA company from Poznan using ATOS Triple Scan. The mentioned system uses a specially developed measuring and projection technology from GOM. Using this brand new technology, the ATOS Triple Scan produces a high accuracy and improved measurement of shiny surface, complete data on complex components with deep pockets or fine edges such as turbine blades, reducing the number of individual scans and resulting in a simple handling. System is also equipped with blue light technology. The narrowband blue light enables precise measurements to be carried out independently of environmental lighting conditions. ATOS uses high resolution measuring cameras with up to 12 megapixel resolution and specially developed optics for precise measurement. The accuracy, measurement resolution and measuring area are completely adaptable to the application requirements. This allows for the highest resolution for highly detailed, small parts with measuring volumes up to 38 mm, or for extremely fast digitizing of large objects with measuring volumes up to 2 m. Measurements were made for eight log points, denoted L1-L8, as shown in Fig.3. The welding voltage was 10V with current 28A and the welding speed was 5 mms^{-1}. The experimental test was repeated five times for the same experimental conditions. In Fig. 4 the example plates after welding are presented.

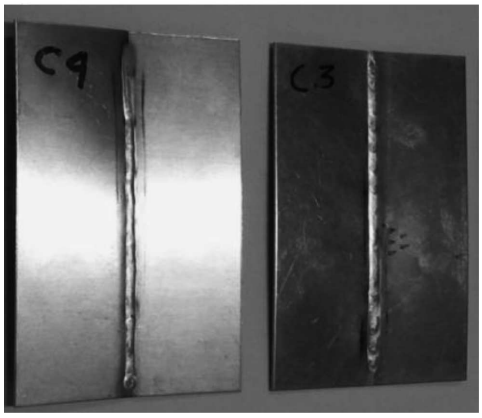

Fig. 4. Example plates after welding process

3. Numerical model

3.1. Numerical methods

In the present work finite element method was used for the simulation. Solution domain was divided into elements of finite size (Fig. 5). The displacement field is defined as the sum of the shape functions multiplied by the displacement value at the associated node.

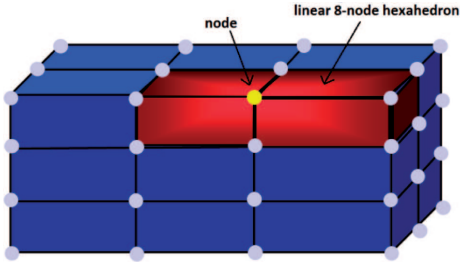

Fig. 5. Solutions domain divided into elements

A large global equation is solved with respect to displacements:

$$Au = b \tag{1}$$

The elastic properties enter into in A. The thermal and plastic strains, as well as the volumetric and surface forces enter into b. The global equation is usually solved by a conjugated gradient method. Time discretization in carried out with a simple differential method. At the first iteration on a time step, an estimate guess on the plastic strains is carried out based on the value in the preceding time step. In the next iterations improved guesses are made from solving the set of non-linear constitutive equations (locally) based on the total strains derived from the displacement field.

3.2. Governing equations

Neglecting mechanical dissipation and assuming equilibrium at the microscopic scale, the transient heat transfer is governed by [7]:

$$\rho c_p \dot{T} + \rho \dot{g} \Delta H = \nabla(\lambda \nabla T) \tag{2}$$

where ρ, c_p, λ, T, ΔH and $\dot{g}$ denote the density, specific heat capacity, thermal conductivity, temperature, latent heat of fusion, and the liquid fraction, respectively. Thermal boundary condition include both convection from Fourier's law and radiation from Stefan-Boltzmann law:

$$-\lambda \frac{\partial T}{\partial n} = h\,(T - T_{air}) + \epsilon\omega(T^4 - T_{air}^4) \tag{3}$$

where h, ϵ, ω and T_{air} denote the heat transfer coefficient, thermal emissivity, Stefan-Boltzmann constant, and ambient air temperature, respectively.

Non-uniform thermal contraction due to density variation with temperature is the cause of the evolution of stresses and deformation. A quasi-static balance is assumed, and the mechanical equilibrium is governed by the Cauchy's equation :

$$\nabla\sigma + \rho g = 0 \tag{4}$$

where σ is the stress tensor, ρ is the density, and g is the body force per unit mass.

In certain metal welded parts, the solid-state austenite-martensite transformation during cooling has a significant influence on the stresses and distortion. When the martensite is formed, the volume of metal is increased, and the transformation plasticity is also produced. For certain metals, to evaluate the residual stress and deformation accurately, phase transformation must be considered.

Therefore, the total strain ε can be decomposed into elastic ε_e, viscoplastic ε_p, thermal ε_{th}, volumetric change ε_{dV} and transformation plasticity ε_{tp}:

$$\varepsilon = \varepsilon_e + \varepsilon_p + \varepsilon_{th} + \varepsilon_{dV} + \varepsilon_{tp} \tag{5}$$

In proposed model (first simply approach) for welding of Inconel 625 alloy the last two components of equation (5) is not taken into account. Ignoring this component, the strain increment can be written as follows:

$$\Delta\varepsilon = \Delta\varepsilon_e + \Delta\varepsilon_p + \Delta\varepsilon_{th} \tag{6}$$

The elastic strain is defined by the temperature dependent Hooke's law, and the volumetric thermal strain is related to temperature:

$$\varepsilon_{th} = \int_T {}_{ref}{}^T \alpha\,(T)\,dT \tag{7}$$

where $\alpha(T)$ is the temperature dependent expansion coefficient, T_{ref} is the reference temperature for zero thermal strain. Below solidus, the material is considered as elastic-viscoplastic, using von Mises yield criterion, and under the assumption of isotropic hardening, the effective viscoplastic strain, $\bar{\varepsilon}_p$, and strain rate, $\dot{\bar{\varepsilon}}_p$, are related to the effective stress, $\bar{\sigma}$, by:

$$\bar{\sigma} = \sigma_Y + k\bar{\varepsilon}_p^n + \dot{\bar{\varepsilon}}_p^m \tag{8}$$

The plastic threshold, σ_Y, the consistency, k, the hardening coefficient, n, and the strain-rate sensitivity coefficient, m, are temperature dependent function given in Table 1. In the absence of flow stress curves for Inconel 625 alloy for the simulations purposes the curve for the stainless steel are used.

TABLE 1

Flow stress coefficients[7]

T, [°C]	n	k	m	σ_Y
20.00	0.6300	1200.00	0.00000	386.000
200.00	0.4500	1200.00	0.01137	305.000
300.00	0.2500	1115.00	0.01768	269.500
330.00	0.2200	1089.50	0.01958	258.850
375.00	0.2500	1051.25	0.02242	242.875
400.00	0.4900	1030.00	0.02400	234.000
425.00	0.7600	991.00	0.02850	207.250
470.00	0.7800	920.80	0.03660	159.100
500.00	0.7300	874.00	0.04200	127.000
600.00	0.4500	718.00	0.06000	20.000
800.00	0.3400	142.00	0.10000	5.000
900.00	0.3300	113.00	0.10500	4.000
1000.00	0.3300	87.00	0.11000	3.000
1100.00	0.3200	68.00	0.12000	2.000
1200.00	0.3100	52.00	0.13000	1.000
1300.00	0.1627	36.00	0.16325	0.000
1400.00	0.0155	20.00	0.19650	0.000
1410.52	0.0000	6.00	0.20000	0.000

3.3. Boundary conditions

The finite element mesh of the investigated model is presented in the Fig. 6. The FEM welding model consists of interior domains and boundary domains (Fig. 6). Interior domains (ID) correspond to base material and filler metal for a single pass weld, whereas, 13 different boundary domains are defined in the model (BID). The mechanical and thermal boundaries are applied into defined boundary domains. In the current configuration, 8-noded hexahedral finite elements were used. As seen in Fig.6 the welding fillet (ID=3) is pre-meshed, but initially these elements are not active (zero density). Only (when the heat input to the elements is sufficient for the liquidation) the elements fed enough heat to liquidize are activated and gain density. The temperature dependent material data, liquidus and solidus temperatures used for the Inconel 625 alloy are obtained from the Special Metals [8]. The convective surface heat transfer coefficient in Eq. (2) was set to 5 $\mathrm{Wm^{-2}K^{-1}}$, with a reference temperature (T_{air}) of 25°C, the emissivity was set to 0.2 [7]. Mechanical boundaries were defined as a distributed spring stiffness normal to surface applied to BID=5,7 and BID=9,11.

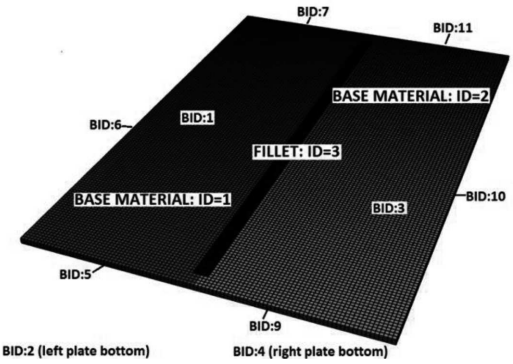

Fig. 6. Welding FEM model with marked Interior Domain (ID) and Boundary Domain (BID)

3.4. Moving heat model

In this work, the Goldak's double-ellipsoid heat flux distribution representing the welding heat source is adopted. As shown in Fig. 7, the heat flux distribution combines two different ellipses. The power densities of the double-ellipsoid heat flux, $q_{v_{if}}(x,y,z,t)$ and $q_{v_{ir}}(x,y,z,t)$, describing heat flux distributions inside the front and rear quadrant of the heat source, can be expressed as [9,10]:

$$q_{v_{if}}(x,y,z,t) = \frac{6\sqrt{3}f_f Q}{abc_f\pi\sqrt{\pi}} e^{-3x^2/c_f^2} e^{-3y^2/a^2} e^{-3z^2/b^2} \tag{9}$$

$$q_{v_{ir}}(x,y,z,t) = \frac{6\sqrt{3}f_r Q}{abc_r\pi\sqrt{\pi}} e^{-3x^2/c_r^2} e^{-3y^2/a^2} e^{-3z^2/b^2} \tag{10}$$

where f_f and f_r denote the heat fraction to the front and rear ellipsoidal, fulfilling the relation

$f_f + f_r = 2$, Q are power input (W) which is calculated from:

$$Q = \vartheta UI \tag{11}$$

where ϑ, U, I are the arc efficiency, the voltage and the current, respectively.

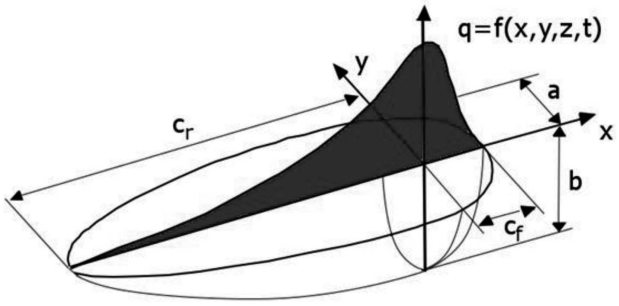

Fig. 7. Illustration of a volume Gaussian double ellipsoidal source, indicating the parameters a, b, c_f, c_r

4. Modelling results and comparison to the experiment

An example of the temperature distribution after 48 seconds of welding and the final effective stress distribution (Von Misses stress) obtained by WeldsimS solver are presented in the Fig. 8 and Fig. 9, respectively. Analysis of the effective stress distribution in welded plates, indicating the formation of the maximum stress at the beginning of the welding process (~250 MPa), which then decreases and reaches a minimum value at the final stage of welding. Dominant stresses in the heat-affected zone (HAZ) are tensile stress (see Fig. 10), which also affect the appearance of the deformation.

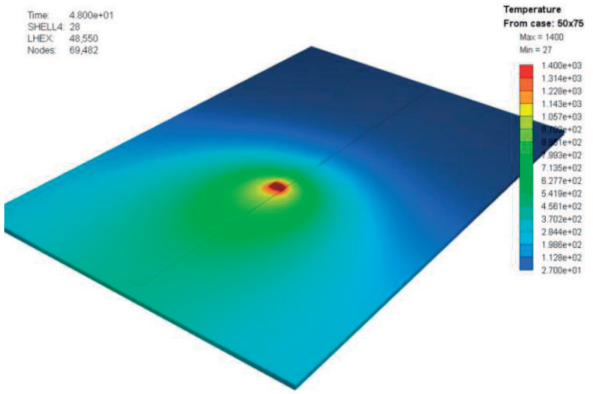

Fig. 8. Temperature distribution at 48 second of the TIG welding process

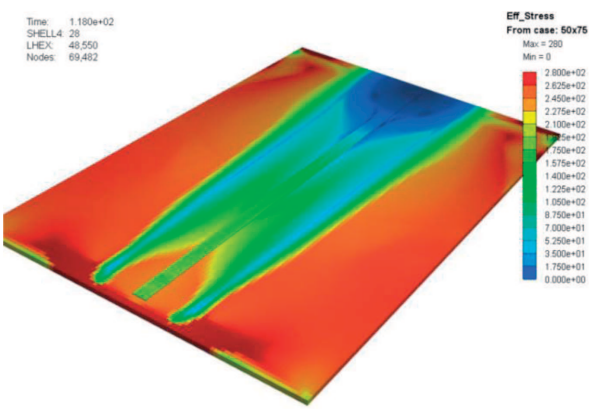

Fig. 9. Effective stress distribution at the final stage of the TIG welding process

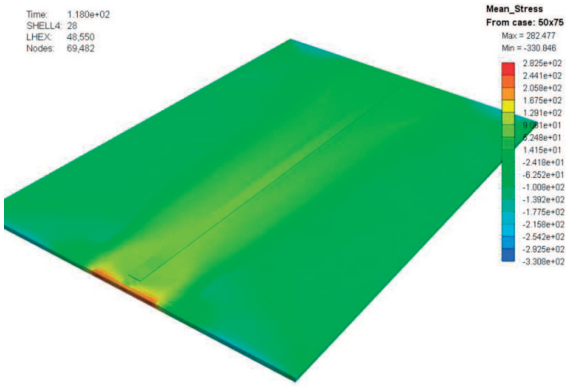

Fig. 10. Mean stress distribution at the final stage of the TIG welding process

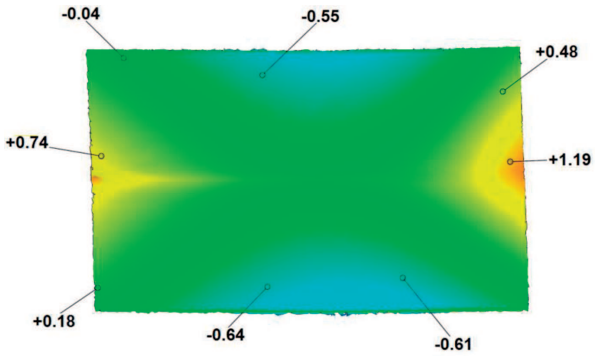

Fig. 11. Distortion in z-direction [mm] measured using ATOS Triple Scan (case no.1)

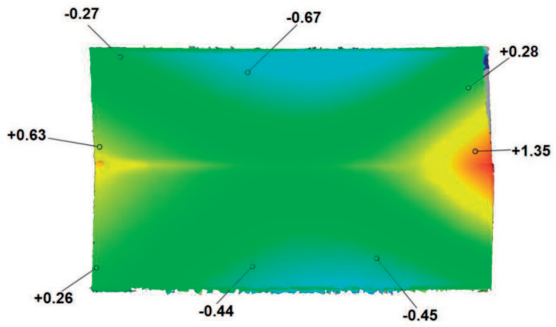

Fig. 12. Distortion in z-direction [mm] measured using ATOS Triple Scan (case no.2)

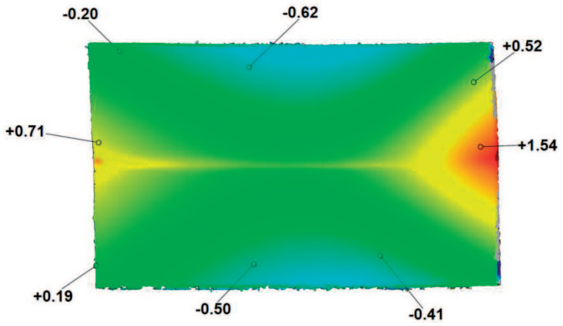

Fig. 13. Distortion in z-direction [mm] measured using ATOS Triple Scan (case no.3)

Fig. 11-13 show examples of the results of measurement of welded plates resulting from the use of 3D scanning system ATOS Triple Scan. The maps show deviations in the z-direction. Analyzing the results, one can observe a similar trend to the formation of deformation for all cases. The maximum deformation (+1.19 mm, +1.35 mm, +1.54 mm) occurs in the area of maximum effective stresses (see Fig. 9).

The comparison of obtained results of distortion in z-direction coming from computer simulations with experimental data for all log points (see Fig. 3) are presented in Fig. 14. The results obtained are characterized by a quite good convergence, despite the use of the strain-stress curves developed for stainless steel. In order to improve the accuracy of deformation calculations, laboratory tests are necessary for right mechanical properties prediction [11,12].

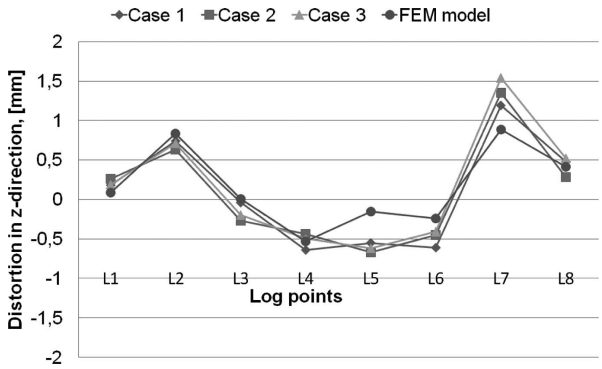

Fig. 14. Experimental results versus computer simulations: distortion in z-direction [mm]

5. Conclusions

In the present work a single pass welding of a Inconel 625 alloy was investigated using FEM solver. Comparison of experimental results with numerical simulations confirms good predictive capabilities of the model. Observed differences (at some log points) between numerical and experimental results indicate the need for more accurate numerical models and material data, especially strain-stress curve for the Inconel 625 alloy for different temperature range and strain rates. Application of the Goldak's heat source model allows for realistic simulation of the TIG welding process. Presented model will be used in further works, which will focus on:

a) application of microstructure sub-model,

b) application of inverse analysis in order to identify chosen parameters of the model,

c) experiments for different kind of heat sources (laser welding) and materials,

d) and finally, industrial validation of the model.

Acknowledgements

The project has been supported by the Polish National Science Centre, Decision number: DEC-2011/03/D/ST8/04041.

REFERENCES

[1] D. Woźniak, M. Głowacki, M. Hojny, T. Pieja, Application of CAE systems in forming of drawpieces with use rubber-pad forming process, Archives of Metallurgy and Materials **57**, 1179 (2012).

[2] Z. Malinowski, M. Rywotycki, Modelling of the strand and mold temperature in the continuous steel caster, Archives of Metallurgy and Materials **9**, 59 (2009).
[3] M. Hojny, Application of an integrated CAD/CAM/CAE/IBC system in the stamping process of a bathtub 1200S, Archives of Metallurgy and Materials **55**, 713 (2010).
[4] J. Bergheau, Y. Vincent, J. Leblond, J. Jullien, Viscoplastic behavior of steels during welding, Science and Technology of Welding and Joining **9**, 323 (2004).
[5] D. Dean, M. Hidekazu, Prediction of welding residual stress in multi-pass welded modified 9Cr-1Mo steel pipe considering phase transformation effects, Computational Materials Science **37**, 209 (2006).
[6] Weldsim reference manual, version 6, November 23 2011.
[7] H.M. Aarbogh, M. Hamide, H.G. Fjaer, A. Mo, M. Bellet, Experimental validation of finite element codes for welding deformations, Journal of Materials Processing Technology **210**, 1681 (2010).
[8] http://www.specialmetal.com
[9] J. Goldak, M. Bibby, J. Moore, R. House, B. Patel, Computer modeling of heat flow in welds, Metallurgical Transactions B **17**, 587 (1986).
[10] J. Goldak, A. Chakravarti, M. Bibby, A new finite element model for welding heat sources, Metallurgical Transactions B **15**, 299 (1984).
[11] M. Głowacki, M. Hojny, Inverse analysis applied for determination of strain-stress curves for steel deformed in semi-solid state, Inverse Problems in Science and Engineering **17**, 159 (2009).
[12] M. Hojny, M. Głowacki, The methodology of strain-stress curves determination for steel in semi-solid state, Archives of Metallurgy and Materials **54**, 475 (2009).

Received: 10 April 2012.